Angle and energy dependence of the superratio for π^+ and π^- elastic scattering from ^{3}H and ^{3}He: Evidence for charge-symmetry violation

C. Pillai,[1,*] D. B. Barlow,[1,*] B. L. Berman,[2] W. J. Briscoe,[2] A. Mokhtari,[2] B. M. K. Nefkens,[1] and M. E. Sadler[3]

[1]*Department of Physics, University of California, Los Angeles, California 90024;*
[2]*Department of Physics, The George Washington University, Washington, D.C. 20052;*
[3]*Department of Physics, Abilene Christian University, Abilene, Texas 79699*

(Received 29 August 1990)

Data are presented on the energy and angle dependence of the charge-symmetry superratio R and simple ratios r_1' and r_2' for $\pi^\pm$ elastic scattering from ^{3}H and ^{3}He. r_1' and r_2' were normalized with respect to $\pi^+ d$ and $\pi^- d$ elastic scattering, which is assumed to have the ratio 1.0. The beam energies are $T_\pi = 142$, 180, and 220 MeV, and the scattering angle, θ_L, ranges from 40° to 110°. In all cases measured it is found that $R > 1$, $r_1' \simeq 1$, and $r_2' > 1$. These results provide substantial evidence for charge-symmetry violation. The angular distributions for $\pi^\pm$ ^{3}H and $\pi^\pm$ ^{3}He elastic scattering also have been measured and comparisons are made with various model calculations.

$$R \equiv \sigma(\theta)[\pi^+ {}^3\mathrm{H}]\sigma(\theta)[\pi^- {}^3\mathrm{H}]/\sigma(\theta)[\pi^- {}^3\mathrm{He}]\sigma(\theta)[\pi^+ {}^3\mathrm{He}],$$

$$r_1' = \sigma(\theta)[\pi^+ {}^3\mathrm{H}]\sigma(\theta)[\pi^- d]/\sigma(\theta)[\pi^- {}^3\mathrm{He}]\sigma(\theta)[\pi^+ d],$$

$$r_2' = \sigma(\theta)[\pi^- {}^3\mathrm{H}]\sigma(\theta)[\pi^+ d]/\sigma(\theta)[\pi^+ {}^3\mathrm{He}]\sigma(\theta)[\pi^- d].$$

I. INTRODUCTION

Elastic scattering of π^+ and π^- from the isospin doublet ^{3}H and ^{3}He provides an interesting way to test the validity of nuclear charge symmetry (CS). Electron elastic scattering on a nucleus is a probe of the spatial distribution of the electric charge, meson-exchange currents, and the spins of the constituent protons and neutrons. But it cannot be applied to probing paired neutrons and, as a consequence, there is a void in our knowledge of the ^{3}H wave function. Elastic pion scattering is eminently suitable for *comparing* the neutron distribution in ^{3}H and the proton distribution in ^{3}He. This is a consequence of $\sigma(\pi^- n) \gg \sigma(\pi^- p)$ in the region of the Δ resonance. To a good approximation we have

$$\sigma(\theta)[\pi^- n \to \pi^- n] \simeq 9\sigma(\theta)[\pi^- p \to \pi^- p] , \tag{1a}$$

and a similar relation holds for its charge-symmetric counterpart

$$\sigma(\theta)[\pi^+ p \to \pi^+ p] \simeq 9\sigma(\theta)[\pi^+ n \to \pi^+ n] . \tag{1b}$$

The comparison of $\sigma(\theta)(\pi^- {}^3\mathrm{H})$ with $\sigma(\theta)(\pi^+ {}^3\mathrm{He})$ is especially sensitive to the difference in the wave functions of the neutron pair in ^{3}H and the proton pair in ^{3}He.

For several reasons, such as the inequality of the coupling constants $g(nn\pi^0) \neq g(pp\pi^0)$, the n-p mass difference, the Coulomb repulsion between the protons in ^{3}He, and the difference in the pp and nn interaction strength, we expect the structures of ^{3}H and ^{3}He to be somewhat different. This implies nuclear charge symmetry breaking (CSB).

In a recent article, Nefkens *et al.*[1] presented a short introduction to CS and CSB. A forthcoming review of the subject can be found in Ref. 2. The modern view holds that the CS operator $\hat{P}_{\mathrm{CS}}$ changes an up into a down quark and vice versa,

$$\hat{P}_{\mathrm{CS}}|\mathrm{up}\rangle = |\mathrm{down}\rangle$$

and (2)

$$\hat{P}_{\mathrm{CS}}|\mathrm{down}\rangle = -|\mathrm{up}\rangle .$$

CSB is then the consequence of the up-down-quark interchange. The quarks differ in mass, electric charge, and magnetic moment. This can manifest itself in small differences in the proton and neutron matter form factors (F_p and F_n) for ^{3}H and ^{3}He. If there was no up-down-quark difference, CS would imply that

$$F_p({}^3\mathrm{H}) = F_n({}^3\mathrm{He}) , \tag{3a}$$

$$F_n({}^3\mathrm{H}) = F_p({}^3\mathrm{He}) . \tag{3b}$$

Furthermore, if CS was valid for the underlying πN interaction, the following relations would hold:

$$\sigma(\theta)[\pi^+ p] = \sigma(\theta)[\pi^- n] , \tag{4a}$$

$$\sigma(\theta)[\pi^- p] = \sigma(\theta)[\pi^+ n] . \tag{4b}$$

The form-factor equalities would imply that the "simple ratios"

$$r_1 = \sigma(\theta)[\pi^+ {}^3\mathrm{H}]/\sigma(\theta)[\pi^- {}^3\mathrm{He}] , \tag{5a}$$

$$r_2 = \sigma(\theta)[\pi^- {}^3\mathrm{H}]/\sigma(\theta)[\pi^+ {}^3\mathrm{He}] \tag{5b}$$

would each be equal to 1.0.

To investigate the precise value of these cross-section ratios, one must have good control of the relative pion beam intensities. This is nontrivial for the intense beams that are required when using gas targets. In Ref. 3 it was pointed out that there is a relation between the four cross sections which can be obtained without knowing the absolute $\pi^{\pm}$ intensity or the detector acceptance, namely, the *superratio*

$$R=\frac{\sigma(\theta)[\pi^{+}\,^{3}\mathrm{H}]\sigma(\theta)[\pi^{-}\,^{3}\mathrm{H}]}{\sigma(\theta)[\pi^{-}\,^{3}\mathrm{He}]\sigma(\theta)[\pi^{+}\,^{3}\mathrm{He}]}$$
$$=r_1 r_2=\frac{\text{yield}(\pi^{+}\,^{3}\mathrm{H})}{\text{yield}(\pi^{+}\,^{3}\mathrm{He})}\frac{\text{yield}(\pi^{-}\,^{3}\mathrm{H})}{\text{yield}(\pi^{-}\,^{3}\mathrm{He})}\,. \tag{6}$$

We define the ratios of the normalized yields as

$$\rho_{+}=\frac{Y(\pi^{+}\,^{3}\mathrm{H}\rightarrow\pi^{+}\,^{3}\mathrm{H})-Y(\pi^{+}bgd)}{Y(\pi^{+}\,^{3}\mathrm{He}\rightarrow\pi^{+}\,^{3}\mathrm{He})-Y(\pi^{+}bgd)}\frac{N(^{3}\mathrm{He})}{N(^{3}\mathrm{H})} \tag{7a}$$

and

$$\rho_{-}=\frac{Y(\pi^{-}\,^{3}\mathrm{H}\rightarrow\pi^{-}\,^{3}\mathrm{H})-Y(\pi^{-}bgd)}{Y(\pi^{-}\,^{3}\mathrm{He}\rightarrow\pi^{-}\,^{3}\mathrm{He})-Y(\pi^{-}bgd)}\frac{N(^{3}\mathrm{He})}{N(^{3}\mathrm{H})}\,. \tag{7b}$$

$N(^{3}\mathrm{H})$ and $N(^{3}\mathrm{He})$ are the number of the $^{3}\mathrm{H}$ and $^{3}\mathrm{He}$ atoms in the targets employed. We see that $R=\rho_{+}\rho_{-}$.

In this paper we present new data on $\pi^{\pm}$ elastic scattering from $^{3}\mathrm{H}$ and $^{3}\mathrm{He}$. In performing these measurements we had the following objectives.

(1) We wanted to improve the original measurement of CSB of Ref. 3, which is fully detailed in Ref. 1. It was found there that R deviates substantially from 1.0. Improvements were made by accumulating good statistics, which were made possible by the use of a more dense gas target and by the use of a new method of $\pi^{\pm}$ beam normalization, based on the near equality of the $\pi^{+}d$ and $\pi^{-}d$ elastic-scattering cross sections.

(2) We wanted to extend the original measurement at $T_{\pi}=180$ MeV to higher and lower pion energies and to larger pion angles. This enables the exploration of the differences in the form factors for $^{3}\mathrm{H}$ and $^{3}\mathrm{He}$ over a larger t interval, where t is the Lorentz invariant four-momentum transfer.

(3) We wanted to test hadron interaction models. Over the years, pion elastic scattering from $^{3}\mathrm{H}$ and $^{3}\mathrm{He}$ has been the subject of many model calculations, performed to determine the trinucleon wave functions, to search for possible three-body interactions, and to investigate hadronic reaction mechanisms.

II. EXPERIMENT

A. The high-pressure gas targets

The high-pressure tritium gas target used in this experiment, shown in Fig. 1, contained 186 kCi of tritium. Five cells for the different gases used in the course of the experiment were utilized. Each cell consists of a thin-walled hollow cylinder, flanged at both ends, that was machined out of a solid block of aluminum. The inside diameter of each cylinder is 12.7 cm, the inside height

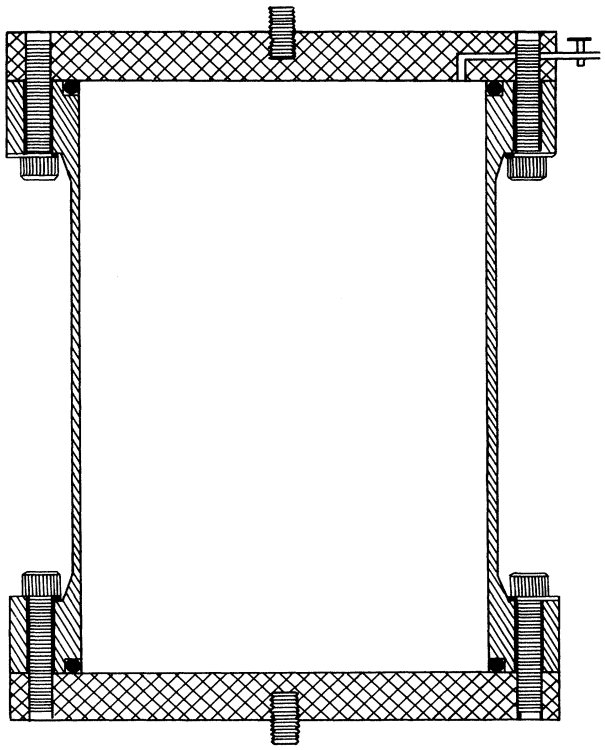

FIG. 1. Cross-sectional diagram of the high-pressure tritium gas cell described in the text. Dimensions are 0.18-cm wall thickness, 18.6-cm inside height, and 12.7-cm inside diameter; the material of the cylinder is aluminum and the end plates are stainless steel.

18.6 cm, and the wall thickness is 0.18 cm. The material is the aluminum alloy 2024-T3511, which was selected because of its high tensile strength (450 MPa) and small diffusion coefficient for tritium. The cylinder is closed on top and bottom by two stainless-steel plates attached to the cylinder by 12 stainless-steel screws and a spring loaded seal buried in a groove 5-mm deep in the end plates. A small channel was drilled through the top plate for the purpose of filling and emptying via a thin supply line welded to the top plate and furnished with a safety lock valve. A 0.635-cm screw could be inserted in the center of the top and bottom plates to attach the cells together in a vertical column. The target cells were tested rigorously for gas leaks by pressurizing them up to 4.8 MPa with helium (and hydrogen in the case of the cell which was to hold the tritium) before being filled. Several extra cells of identical fabrication were pressurized to their yield and rupture points.

The target ladder at the Energetic Pion Channel and Spectrometer[4] (EPICS) was modified to accommodate the five targets arranged in a vertical column. The thick top and bottom plates of the target cells provided rigid surfaces for connecting the cells to each other; they also acted as heat sinks to dissipate the heat generated in the tritium target cell.

The masses of high-pressure gas samples were deter-

mined by direct weighing, and verified by pressure, volume, and temperature (PVT) measurements. The cells were filled and weighed just prior to the experiment and weighed again just afterwards (six weeks later). Each empty cell, approximately 8 kg in mass, was weighed shortly before filling. A 50-kg Voland balance was used which is rated for an absolute accuracy of ±73 mg (per weighing) for a three-sigma (96%) confidence level for masses up to 20 kg. By exercising great care and repeating each weighing and the zero calibration several times, we achieved a precision repeatable to within ±20 mg (in the worst case). Uncertainties in corrections for the air buoyancy (2–12 mg) were small, since the barometric pressure, ambient air temperature, and relative humidity were monitored during the mass measurements. The sample masses determined by direct weighing are known to within ±0.3%.

During the filling process, the sample masses were determined independently from PVT measurements. An additional PVT determination was made for the tritium sample subsequent to the experiment. The pressures were measured with a Heise 40.64-cm gauge, 7.5 MPa full scale, having an absolute accuracy of 0.1%, repeatability of 0.02%, and sensitivity of 0.01%. Thus, the pressures of approximately 3 MPa were measured to ±0.003 MPa. The approximately 2.5-liter volumes were determined precisely by a gas-displacement technique using ^{4}He to ±0.1 cm^3 relative precision and to ±0.8-cm^3 absolute accuracy (the room temperature was controlled to 0.1 °C). In addition, the sample-container dimensions (diameter and length) were measured with vernier calipers to ±0.0025 cm both at 1 atm and at the operating pressure. The temperature was measured during the filling process, using two kinds of thermometers, at several points on each sample container. Particularly, the one containing tritium, whose heat output raised its temperature by several degrees, was carefully checked. The resulting average-temperature measurements were accurate to ±0.05 °C for ^{3}He, ^{1}H, and ^{2}H, and ±0.3 °C for ^{3}H. The number of amagats (moles/molar volume) of the samples ranged from 27.80 (for ^{2}H) to 28.14 (for ^{1}H). The results of the PVT measurements, in themselves nominally accurate to within 0.5%, agreed with those from direct weighing to within 0.3% for ^{3}H and ^{3}He, 1.0% for ^{1}H, and 0.7% for ^{2}H. We regard these measurements to have confirmed those from direct weighing and have used the latter in our cross-section determinations.

The isotopic abundances of the ^{3}H, ^{1}H, and ^{2}H samples were each 99% or higher. That of the ^{3}H sample was measured by mass spectroscopy twice (to within ±0.15%) before the experiment, and much more accurately (to within ±0.01%) afterwards; the two measurements were in agreement within the limits quoted. From this measurement and from the known half-life, a ^{3}H abundance of 98.80±0.01 mol % was determined for the beginning of the experimental run. The major impurities were 1.06±0.05 mol % ^{2}H and 0.14±0.07 mol % ^{1}H. The ^{3}H decays to ^{3}He at the rate of 1.54×10^{-4}/day (approximately 0.5%/month); this was taken into account in the analysis. We use an *average* ^{3}H abundance value during the experiment of 98.47 mol % with an average ^{3}He abundance of 0.33 at. %. The atomic abundance ratios include the accounting for the small differences (less than 0.05%) in the dimensions at operating pressure.

The high radioactivity of the sample involved in this experiment necessitated the use of a special Tritium Enclosure and Vent/Recapture System, radiation monitors, and an independent alarm and interlock systems; a back-up diesel generator (in case of power failure) was kept nearby on standby status. Details of this system can be found in the Safety Operation Procedure Report produced for this experiment.[5]

B. Data acquisition

The experiment was performed using the Energetic Pion Channel and Spectrometer at the Clinton P. Anderson Meson Physics Facility (LAMPF) at $T_\pi=142$, 180, and 220 MeV and at $\theta_L=40°$, 60°, 80°, 90°, and 110°. EPICS has several characteristics that are desirable for these measurements: a large pion flux up to 10^7 π^-/s and 10^8 π^+/s, good energy resolution (500 keV during this experiment), and a large acceptance (about 2% during this experiment). These factors enabled us to measure the elastic-scattering ratios with high precision. The standard EPICS-MP-10 electronics and data-acquisition systems were used to record the data on magnetic tape. The EPICS facility is described in Ref. 4.

Beam monitoring was accomplished using two ionization chambers. One, located 85-cm downstream of the target, monitored the pion beam, and the other monitored the incident proton beam that produced the pions. Furthermore, we used a pair of scintillator telescopes located about 2-m downstream of the target to monitor the muons from pion decay. These devices provided the means by which the relative rates of the π^+ and π^- beams were monitored to better than 1%. Absolute pion fluxes were not measurable directly; the beams contained pions, muons (from π decay), electrons, and protons in amounts that depended on beam species, energy, and channel tuning. The cross-section measurements were made relative to π^+ and π^- elastic scattering on deuterium and/or hydrogen. This method eliminated the need for the determination of the solid angle and acceptance of the spectrometer; all ratios were measured under identical kinematical conditions. The measurements required only that the beam and spectrometer characteristics be kept constant during each run cycle.

The procedures that were followed for data taking were determined by the twofold goals of the experiment: (i) measuring the various cross-section ratios R, r'_1, r'_2, ρ_+, and ρ_- (the primes in r'_1 and r'_2 indicate that the ratios are measured with respect to $\pi^\pm d$ elastic scattering) and (ii) obtaining the absolute differential cross sections. At each angle we successively measured the π^+ yield from ^{3}H, ^{3}He, ^{2}H, ^{1}H, and the empty-target cell with the spectrometer tuned for pion-tritium kinematics, yielding the ratio ρ_+. The accuracy of the ratio of the yields depends on (a) the monitoring of the relative beam flux for all runs that involve the same pion species, (b) the proper determination of the background subtraction (discussed

below), (c) the knowledge of the partial pressures of the ^{3}He and ^{3}H samples, and (d) the spatial stability of the pion beam on the target.

Each measurement of ρ_+ was followed by data collection for the hydrogen, deuterium, and empty targets with the spectrometer tuned for πd kinematics. A comparison of these data with the known hydrogen and deuterium cross sections allows us to normalize to either of these quantities and thus to obtain the cross sections for ^{3}H and ^{3}He. This comparison requires knowledge of the partial pressure of ^{1}H or ^{2}H. We then made a second background determination and checked the overall experimental uncertainty of the $\pi^+ p$ or $\pi^+ d$ cross section being used for normalization.

The above sequence was repeated with the π^- beam, with the same kinematics, to obtain ρ_-. The uncertainty in determining ρ_-, except for the determination of the partial-pressure ratio, is independent of the determination of ρ_+. The superratio is obtained as the direct product $R = \rho_+ \rho_-$.

At several angles and energies some runs were taken with the spectrometer set for πd kinematics. As mentioned above, the differential cross sections were determined by using the known cross sections for pion elastic scattering on deuterium and hydrogen for normalization. In the case of deuterium, the π^+ and π^- cross sections are assumed to be the same, and the difference in yield between the π^+ and π^- scattering from deuterium is therefore merely a measure of the relative π^+/π^- beam flux. In the case of the hydrogen target, the cross sections obtained are only as accurate as the measurements to which we normalize. A complete set of measurements was not taken for the π^- beams at the πd setting. The determination of the π^- cross sections can be made with a smaller uncertainty using the π^+ cross section and r_1'. For this purpose the $\pi^{\pm} d$ measurements made at tritium kinematics were used as a measure of the relative π^+/π^- beam flux.

III. DATA REDUCTION AND RESULTS

Missing-mass histograms were obtained using the momentum and the direction of each scattered particle as measured in the spectrometer and assuming the two-body kinematics of pion elastic scattering for each event. As a result of the loss of a plane of the front wire chamber in the focal plane, the energy resolution of the missing-mass spectra had deteriorated somewhat. Software cuts were applied to the histograms of the target projections ($X_{\rm tgt}$, $Y_{\rm tgt}$, $\theta_{\rm tgt}$, and $\phi_{\rm tgt}$), Ref. 4, to reduce the background. Many muons from pions that decayed inside the spectrometer magnet were rejected upon comparing the angles measured at the front of the spectrometer and at the position of the focal plane.

The data analysis was divided into two parts: (1) the evaluation of the relative yields to calculate the superratio and simple ratios and (2) the determination of the total yields for the absolute cross sections. For part (1), the relative yields from the ^{3}H, ^{3}He, ^{2}H, and empty targets are sufficient as long as they are calculated in a consistent manner. The yield from a particular target is obtained from the number of counts in the elastic peak of the missing-mass spectrum; our definition of the peak typically includes 95% of the counts. The peak integral is multiplied by a normalization factor which depends on the chamber efficiency, survival factor of the pions in the spectrometer, number of particles recorded by one of the ion chambers, and the computer live time.

At most angles and energies, we have data for the same target that was obtained at different times to check for consistency. Occasionally a shift in the centroid of the elastic peak was observed. In a few cases this could be attributed to a small change in the current of the quadrupole magnet in the beam transport system. The number of channels shifted was determined by subtracting one normalized spectrum from another to obtain the difference spectrum. If the spectra were perfectly matched, the difference spectrum should be zero. All the spectra were thus checked and, if necessary, shifted to align with a "standard" run.

For the background measurements we used the hydrogen, the empty, and sometimes the deuterium targets. Several determinations of the background were necessary since the spectra obtained after either hydrogen or empty-cell background subtraction revealed a residual background that was proportional to the area of the elastic peak (about 2 and 3 % for the hydrogen and empty-cell background determinations, respectively). This residual background comes from muons from pion decay and from doubly scattered pions. While the main source of background is the cell wall, the five cells contained different amounts of target material, each of a different mass; therefore the pion energy loss and multiple scattering are note equal for the five targets. Thus, it was important not to rely on a background determination based solely on one target. The deuterium yield is an attractive candidate for background subtraction because deuterium duplicates more closely tritium and ^{3}He with respect to energy loss and nuclear scattering and it has the same scattering cross section for π^+ and π^-, which is not the case for hydrogen. However, at forward angles it could not be used due to the proximity of the deuterium elastic peak to the peaks of interest, as illustrated in Fig. 2(a). Also, the need to accurately evaluate the tail of the deuterium peak that extends under the $A=3$ peak makes the background subtraction unreliable for this case. The hydrogen and empty-target spectra did not have these problems, as can be seen in Figs. 2(b) and 2(c).

Generally, we did not obtain data on hydrogen with hydrogen kinematics and thus corrections had to be made for the acceptance variation of the spectrometer for noncentral momenta. This correction factor was determined during the development period immediately preceding data taking. In those cases where the relative efficiency was below 50%, we used only the deuterium peak for beam normalization. A weighted average and the standard deviation for the normalized yield (Y) of different runs were calculated for each target at each angle and energy. The standard deviation gives a measure of the run to run consistency, which was better than 2% for all cases. The yield of the background target was cal-

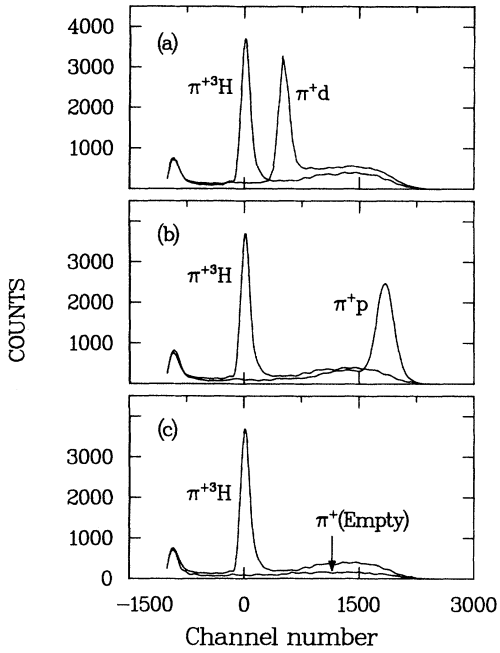

FIG. 2. (a) Two typical missing-mass spectra for $T_\pi = 142$ MeV and $\theta_{lab} = 60°$. The results obtained with the tritium and deuterium targets have been superimposed. (b) Same as (a) for the tritium and hydrogen targets. (c) Same as (a) for the tritium and empty targets.

culated for the same energy interval as the main peak. This procedure was used for all targets and for both π^+ and π^- runs. The use of different background targets (empty, hydrogen, and deuterium) had little effect (less than 2%) on the values of ρ_+ and ρ_-. The values of ρ_+ and ρ_- as a function of the laboratory angle for our three incident energies are listed in Table I and plotted in Fig. 3. The superratio R is obtained as the direct product of ρ_+ and ρ_- and is independent of the absolute π^+ and π^- beam fluxes. The results for the superratio are given in Table II where we have included the value of the four-momentum transfer $-t$ for each energy and angle. These data are displayed in Fig. 4. The error bars shown are statistical only.

The pion flux at EPICS is usually calibrated with the help of $\pi^+ p$ elastic scattering. This method is not suitable for a π^- beam on a gas target because of the small $\pi^- p$ cross section, since

$$\sigma(\theta)[\pi^- p] \simeq \tfrac{1}{9}\sigma(\theta)[\pi^+ p] \ .$$

Also, there is some controversy over the reference value for $\sigma(\theta)[\pi^- p]$ given by different πN partial-wave analyses. Instead, we use $\pi^{\pm} d$ elastic scattering for the relative beam calibrations. The TRIUMF work on $\pi^{\pm} d$ scattering[6] shows that $\sigma(\theta)[\pi^+ d]$ is equal to $\sigma(\theta)[\pi^- d]$ to within a few percent at the energies and angles of interest here. The charge-symmetric simple ratios

$$r_1' = \frac{\sigma(\theta)[\pi^+ {}^3\mathrm{H}]}{\sigma(\theta)[\pi^- {}^3\mathrm{He}]} \frac{\sigma(\theta)[\pi^- d]}{\sigma(\theta)[\pi^+ d]} \tag{8a}$$

and

$$r_2' = \frac{\sigma(\theta)[\pi^- {}^3\mathrm{H}]}{\sigma(\theta)[\pi^+ {}^3\mathrm{He}]} \frac{\sigma(\theta)[\pi^+ d]}{\sigma(\theta)[\pi^- d]} \tag{8b}$$

are marked with a prime to denote that the normalization of the π^+ and π^- beams is based on πd elastic scattering. When CS is valid, these ratios must be equal to one. The advantage of using r_1' and r_2', rather than the ratio of the absolute cross sections, is the superior experimental accuracy, since they do not depend on the absolute π^+ and π^- beam normalizations. The results for these "primed" charge-symmetric simple ratios are also given in Table I and displayed in Fig. 5. The systematic uncertainty in the simple ratios is less than 4%, mainly governed by the uncertainty in our measured $\pi^{\pm} d$ yields.

The second part of the data analysis was the determination of the absolute differential cross sections. For this determination the absolute yield from each target

TABLE I. The cross-section ratios ρ_+ and ρ_-, the charge-symmetric simple ratios r_1' and r_2', and the superquotient Q. The error limits for Q do not include the uncertainties in the π^+ and π^- beam calibrations.

Energy (MeV)	θ_π (lab) (deg)	r_1'	r_2'	ρ_+	ρ_-	$Q = r_2'/r_1'$
142	40	1.021±0.027	1.060±0.029	0.617±0.016	1.754±0.028	1.04±0.04
	60	1.041±0.030	1.079±0.030	1.054±0.014	1.066±0.017	1.04±0.04
	80	1.007±0.046	1.143±0.050	1.045±0.024	1.102±0.027	1.14±0.07
	90	1.038±0.069	1.106±0.065	0.689±0.019	1.666±0.068	1.07±0.09
	110	0.997±0.045	1.107±0.044	0.607±0.015	1.818±0.052	1.11±0.07
180	40	0.998±0.022	1.087±0.025	0.676±0.009	1.604±0.021	1.09±0.04
	60	1.002±0.025	1.183±0.031	1.392±0.021	0.851±0.016	1.18±0.04
	80	1.000±0.040	1.126±0.047	1.388±0.030	0.812±0.022	1.13±0.07
	110	1.020±0.068	1.159±0.072	0.863±0.020	1.371±0.056	1.14±0.10
220	40	1.033±0.026	1.107±0.026	0.789±0.015	1.450±0.024	1.07±0.04
	60	1.042±0.038	1.109±0.045	1.675±0.047	0.690±0.018	1.07±0.06
	80	0.976±0.084	1.283±0.123	1.657±0.122	0.755±0.057	1.31±0.20

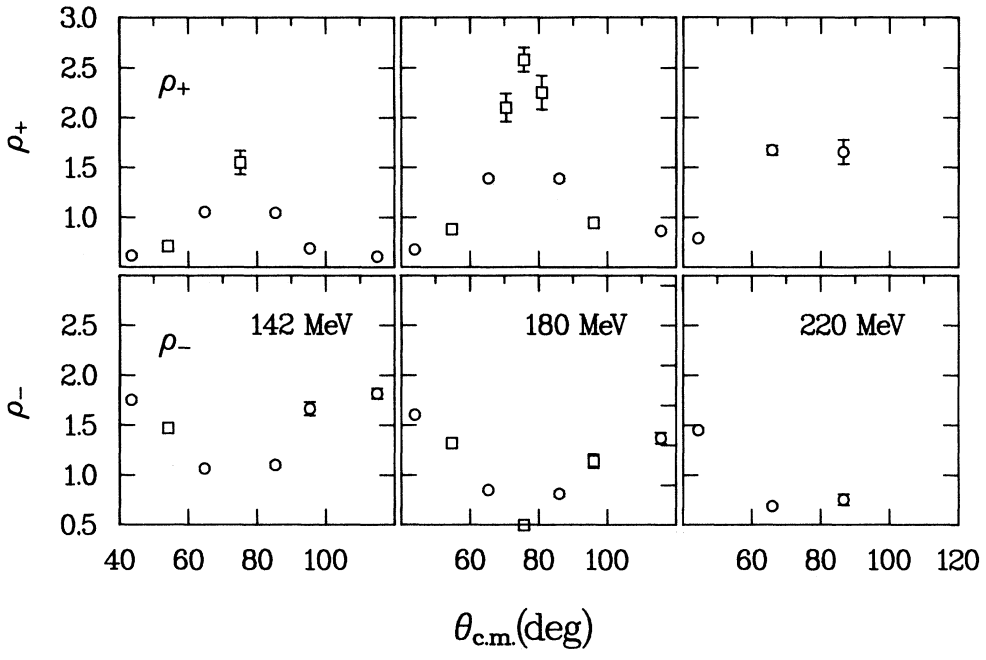

FIG. 3. The ratios of the cross sections $\rho_+ = \sigma(\theta)[\pi^+ {}^3\mathrm{H}]/\sigma(\theta)[\pi^+ {}^3\mathrm{He}]$ and $\rho_- = \sigma(\theta)[\pi^- {}^3\mathrm{H}]/\sigma(\theta)[\pi^- {}^3\mathrm{He}]$. The circles are the present results. The squares are the results from Ref. 1.

was obtained, using the complete peak areas. The residual background, after the background subtraction, was approximately 2–3 % for all cases. For the determination of the absolute differential cross section this extra background was subtracted. When calculating the yields from the deuterium target for normalization, care was taken not to include breakup events in the elastic peak. Our procedure could be verified in a few cases by calculating the differential cross section for $\pi^+ d$ using as beam normalization $\pi^+ p$ based on the Virginia Polytechnic Institute and State University (VPI) cross sections[7] and then comparing our πd results to the Swiss Institute for Nuclear Research (SIN) data.[8] These results are given in Table III. Note that a change in the π^-/π^+ normalization affects r_1' and r_2' in opposite ways.

The differential cross sections for π^+ elastic scattering on ^{3}H and ^{3}He were obtained by calibrating the π^+ beam using the $\pi^+ d$ elastic-scattering data from SIN,[8] which is

TABLE II. The superratio R.

Energy (MeV)	θ_π (c.m.) (deg)	θ_π (lab) (deg)	R	$-t$ (fm^{-2})
142	43.5	40	1.082±0.039	0.70
	64.7	60	1.123±0.038	1.46
	85.3	80	1.152±0.061	2.35
	95.4	90	1.148±0.086	2.80
	115.0	110	1.104±0.064	3.62
180	44.0	40	1.084±0.039	0.97
	65.3	60	1.185±0.036	2.01
	85.9	80	1.127±0.057	3.21
	115.6	110	1.183±0.078	4.93
220	44.4	40	1.144±0.037	1.28
	65.9	60	1.156±0.055	2.65
	86.6	80	1.251±0.121	4.21

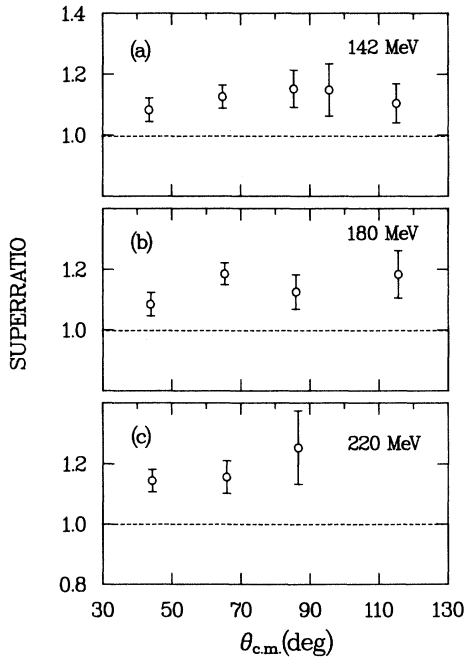

FIG. 4. The superratio R at $T_\pi = 142$, 180, and 220 MeV. The dashed line at $R = 1.0$ is the prediction when CS is valid.

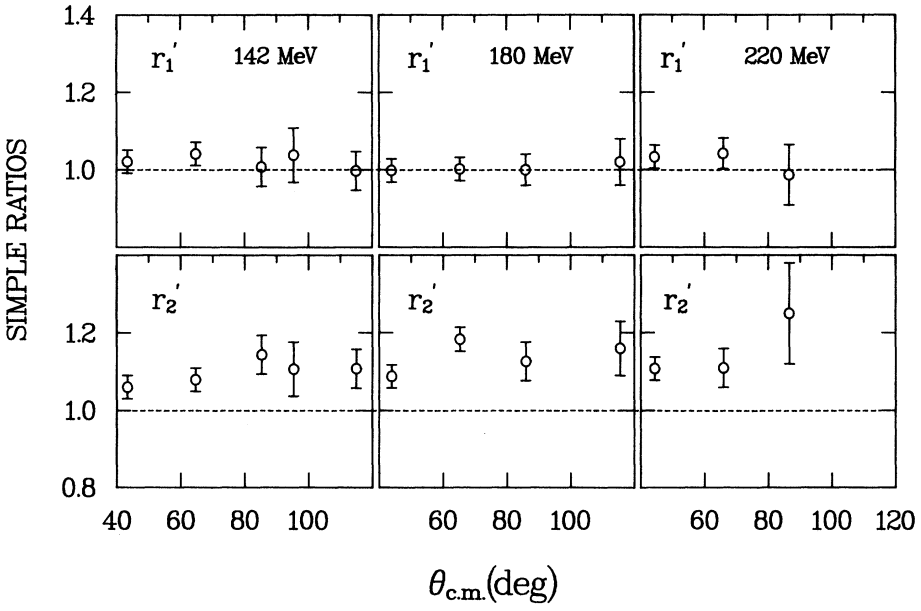

FIG. 5. The charge-symmetric ratios r_1' and r_2'. CS implies $r_1'=r_2'=1$; this is shown by the dashed lines at $r=1.0$.

reported to have an absolute accuracy of 5%. To obtain the π^- cross section, we assume that

$$r_d=\sigma(\theta)[\pi^+ d\to\pi^+ d]/\sigma(\theta)[\pi^- d\to\pi^- d]=1.0\ .$$

At our energies, r_d has been found to deviate from one by less than 4%.[6] The results for the differential cross sections are given in Table IV together with the πd data used for calibration. Figure 6 shows the angular distribution for π^+ ^{3}H and π^- ^{3}H elastic scattering.

The superratio is obtained as the direct product of ρ_+ and ρ_-, which are independent of the absolute beam normalization and detector efficiency. Most of the systematic uncertainties cancel to first order in the superratio. The main systematic error comes from the uncertainty in the ratio of the number of ^{3}H to ^{3}He atoms. As mentioned above, this ratio was determined to within 0.3% accuracy. The effect of this systematic error is to change all values of R uniformly by $2\times0.3=0.6\%$. Preliminary results of our experiment have already appeared as Ref. 10; the present values supersede these.

TABLE III. Comparison of $\pi^+ d$ elastic-scattering cross sections with published data and input $\sigma(\theta)[\pi^+ p\to\pi^+ p]$ values.

Pion energy (MeV)	θ_{lab} (deg)	$\sigma(\theta)[\pi^+ d]$ c.m. this work (mb/sr)	$\sigma(\theta)[\pi^+ d]$ c.m. existing[a] (mb/sr)	$\sigma(\theta)[\pi^+ p]$ c.m. input (mb/sr)
142	40	9.40±0.33	9.62±0.80	17.0
180	40	10.40±0.63	10.50±0.80	27.3
220	40	7.07±0.43	7.00±0.40	23.6

[a]From Ref. 8.

IV. ANALYSIS

A. Comparison with previous experiment

$\pi^\pm$ elastic-scattering data on ^{3}H and ^{3}He at $T_\pi=143$ and 180 MeV have been obtained previously by the University of California, Los Angeles (UCLA) group[1] using a

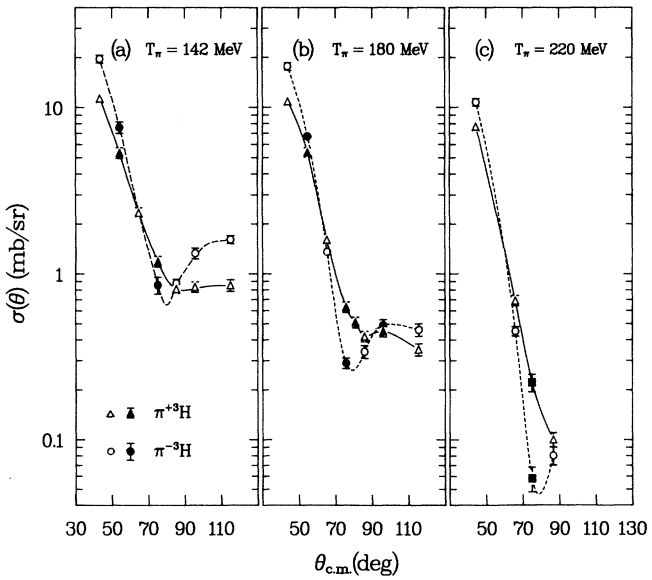

FIG. 6. (a) Differential cross sections in the center-of-mass system for π^+ and π^- elastic scattering from ^{3}H for $T_\pi=142$ MeV. The curves are drawn to guide the eye. The solid symbols are data points from Ref. 1. (b) Same as (a) for $T_\pi=180$ MeV. (c) Same as (a) for $T_\pi=220$ MeV. The solid data points at 75° in the NSF dip region are from a recent experiment by our group.

TABLE IV. Differential cross sections $\sigma(\theta)$ in the center-of mass system.

θ_π (lab) (deg)	$\pi^+ {}^3$H (mb/sr)	$\pi^- {}^3$H (mb/sr)	$\pi^+ {}^3$He (mb/sr)	$\pi^- {}^3$He (mb/sr)	πd[a] (mb/sr)
			$T_\pi=142$ MeV		
40	11.36±0.63	19.64±1.09	18.41±1.02	11.24±0.62	9.62±0.50[b]
60	2.34±0.18	2.36±0.19	2.22±0.17	2.22±0.18	2.60±0.20[b]
80	0.81±0.05	0.88±0.05	0.78±0.05	0.80±0.05	1.28±0.06[b]
90	0.83±0.07	1.33±0.11	1.21±0.09	0.80±0.07	1.24±0.09[c]
110	0.87±0.07	1.61±0.14	1.44±0.12	0.88±0.08	1.11±0.09[c]
			$T_\pi=180$ MeV		
40	10.88±0.55	17.71±0.88	16.11±0.81	11.12±0.55	10.50±0.50[b]
60	1.63±0.08	1.36±0.08	1.18±0.07	1.59±0.09	2.00±0.10[b]
80	0.43±0.03	0.35±0.02	0.31±0.02	0.43±0.03	0.70±0.03[b]
110	0.35±0.03	0.46±0.04	0.40±0.02	0.34±0.02	0.53±0.03[c]
			$T_\pi=220$ MeV		
40	7.66±0.45	10.73±0.62	9.51±0.56	7.44±0.45	7.00±0.40[b]
60	0.69±0.05	0.45±0.04	0.41±0.03	0.65±0.05	0.95±0.04[b]
80	0.097±0.006	0.076±0.005	0.059±0.005	0.101±0.008	0.23±0.01[b]

[a]Used for normalization.
[b]From Ref. 8.
[c]From Ref. 9.

smaller gas target. The comparison of the previous data, using $\pi^{\pm}p$ data for calibration, with the present result based on $\pi^{\pm}d$ measurements for calibration is made in Tables V and VI. The agreement between the two data sets, on the whole, is very good.

B. Violation of charge symmetry

In the relativistic impulse approximation discussed in Ref. 1, the differential cross sections for $\pi^+ {}^3$H and $\pi^- {}^3$H elastic scattering up to $\theta_\pi \simeq 90°$ in c.m. are given by

$$\sigma(\theta)[\pi^+ {}^3\mathrm{H}]=a_+^2\,|F_p({}^3\mathrm{H})|^2\{|[1+\tfrac{2}{3}\alpha_t({}^3\mathrm{H})]f|^2+|g|^2\}\ , \tag{9a}$$

$$\sigma(\theta)[\pi^- {}^3\mathrm{H}]=a_-^2\,|F_p({}^3\mathrm{H})|^2\{|[\tfrac{1}{3}+2\alpha_t({}^3\mathrm{H})]f|^2+\tfrac{1}{9}|g|^2\}\ , \tag{9b}$$

where a_+ and a_- are the medium coefficients, F_p and F_n are the proton and neutron matter form factors for ^{3}H, f is the π^+p non-spin-flip scattering amplitude, and g is the spin-flip scattering amplitude. We have used the Δ-dominance relations for πN scattering that are applicable in the region of the $\Delta(1232)$, namely,

$$3f(\pi^+n)\simeq f(\pi^+p)=f(\pi^-n)\simeq 3f(\pi^-p)$$

and

$$3g(\pi^+n)\simeq g(\pi^+p)=g(\pi^-n)\simeq 3g(\pi^-p)\ .$$

For the numerical calculations reported below, we use the exact values for f and g obtained from the VPI $\pi^{\pm}p$ partial-wave analysis; finally, we use $a_+({}^3\mathrm{H})=0.86$ and $a_-({}^3\mathrm{H})=0.82$, as discussed in Ref. 1. The neutron and proton matter form factors are related by

$$F_n({}^3\mathrm{H})=\alpha_t({}^3\mathrm{H})F_p({}^3\mathrm{H})\ . \tag{10a}$$

The charge-symmetric expressions for the ^{3}He matter form factor is

TABLE V. Comparison of the cross-section ratios ρ_+ and ρ_- and the simple ratios r_1' and r_2' of this work with those of Ref. 1, presented as ratios of the present data to those of the previous experiment.

T_π (MeV)	θ_π (lab) (deg)	ρ_+ (present) / ρ_+ (Ref. 1)	ρ_- (present) / ρ_- (Ref. 1)	r_1' (present) / r_1 (Ref. 1)	r_2' (present) / r_2 (Ref. 1)
142	40	0.98±0.03	1.01±0.04	0.98+00.06	1.02±0.05
	60	1.03±0.03			0.96±0.08
180	40	0.98±0.03	1.03±0.04	0.96±0.04	1.05±0.04
	60	1.02±0.03	0.94±0.06	0.93±0.06	1.01±0.06
	80	1.02±0.06	0.98±0.07	0.97±0.07	1.04±0.09

TABLE VI. Comparison of differential cross sections with those of Ref. 1, presented as ratios of cross sections of this experiment to those of the previous experiment.

T_π (MeV)	θ_π (lab) (deg)	π^+ ^{3}H $\frac{\sigma(\theta)\text{ (this work)}}{\sigma(\theta)\text{ (Ref. 1)}}$	π^- ^{3}H $\frac{\sigma(\theta)\text{ (this work)}}{\sigma(\theta)\text{ (Ref. 1)}}$	π^+ ^{3}He $\frac{\sigma(\theta)\text{ (this work)}}{\sigma(\theta)\text{ (Ref. 1)}}$	π^- ^{3}He $\frac{\sigma(\theta)\text{ (this work)}}{\sigma(\theta)\text{ (Ref. 1)}}$
142	40	1.02±0.07	1.07±0.07	1.04±0.07	1.05±0.08
	60	0.96±0.07	0.94±0.10	0.93±0.10	
180	40	0.93±0.06	1.01±0.06	0.95±0.06	0.98±0.06
	60	0.95±0.06	0.93±0.08	0.94±0.08	0.99±0.08
	80	0.96±0.07	0.97±0.10	0.94±0.10	0.98±0.08

$$F_p(^3\text{He})=\alpha_t(^3\text{He})F_n(^3\text{He})\ . \tag{10b}$$

In the region of the non-spin-flip (NSF) dip, Ref. 1, where $f/g<1$, which is near $\theta_{\text{c.m.}}=78°$ for $T_\pi=180$ MeV, we have

$$r_1'=\left|\frac{F_p(^3\text{H})}{F_n(^3\text{He})}\right|^2\left|\frac{g(\pi^+p)}{g(\pi^-n)}\right|^2\frac{\sigma(\theta)[\pi^-d]}{\sigma(\theta)[\pi^+d]}$$
$$\simeq\left|\frac{F_p(^3\text{H})}{F_n(^3\text{He})}\right|^2\ . \tag{11}$$

CSB can be parametrized by β_t, which is the ratio of the odd-nucleon form factors

$$\beta_t\equiv F_p(^3\text{H})/F_n(^3\text{He})\ . \tag{12}$$

$\beta_t\neq1$ implies CSB. The parameter β_t depends only on t. The r_1' data given in Table I result in the values for β_t of Table VII, covering the interval in four-momentum transfer from -1.5 to -4.2 fm^{-2}. There is no evidence for CSB within the 3% experimental uncertainty in our comparison of the *odd*-nucleon form factors for ^{3}H and ^{3}He. We can summarize the results of Table VII as

$$F_p(^3\text{H})=(1.00\pm0.03)F_n(^3\text{He}) \tag{13}$$

for $1.5\text{ fm}^{-2}<-t<4.2\text{ fm}^{-2}$. Outside the NSF region we have

$$r_2'\simeq\left|\frac{F_n(^3\text{H})}{F_p(^3\text{He})}\right|^2\ . \tag{14}$$

CSB also can be parametrized by γ_t, the ratio of the even-nucleon form factors,

$$\gamma_t\equiv F_n(^3\text{H})/F_p(^3\text{He})\ . \tag{15}$$

TABLE VII. Results for the CSB parameter β_t, the ratio of the odd-nucleon form factors: $\beta_t\equiv F_p(^3\text{H})/F_n(^3\text{He})$.

$-t$ (fm^{-2})	β_t	T_π (MeV)	θ_π (lab) (deg)	θ_π (c.m.) (deg)
1.5	1.02±0.03	142	60	64.7
2.0	1.00±0.03	180	60	65.3
2.4	1.00±0.03	142	80	85.3
2.7	1.02±0.03	220	60	65.9
3.2	1.00±0.03	180	80	85.9
4.2	0.99±0.04	220	80	86.6

$\gamma_t\neq1$ implies CSB. Our results are shown in Table VIII for the range of four-momentum transfer from -0.3 to -4.9 fm^{-2}. Here the data can be summarized as

$$F_n(^3\text{H})=[1.00+(0.02\pm0.01)|t|\,]F_p(^3\text{He})\ . \tag{16}$$

This summary is based on the value $F=1.00$ at $t=0$ (required by the definition of the form factor) and on $F=\exp(-\beta t)$ discussed in Ref. 1.

The superquotient of cross sections, defined in Ref. 1,

$$Q=\frac{\sigma(\theta)[\pi^-\,^3\text{H}]}{\sigma(\theta)[\pi^+\,^3\text{He}]}\frac{\sigma(\theta)[\pi^-\,^3\text{He}]}{\sigma(\theta)[\pi^+\,^3\text{H}]}=\frac{r_2'}{r_1'} \tag{17}$$

becomes, outside the NSF dip region,

$$Q=\left|\frac{\frac{1}{3}+2\alpha_t(^3\text{H})}{\frac{1}{3}+2\alpha_t(^3\text{He})}\right|^2\left|\frac{1+\frac{2}{3}\alpha_t(^3\text{He})}{1+\frac{2}{3}\alpha_t(^3\text{H})}\right|^2\ . \tag{18}$$

CSB also can be parametrized by the relation

$$\alpha_t(^3\text{H})=(1+\varepsilon_t)\alpha_t(^3\text{He})\ , \tag{19}$$

where $\varepsilon_t\neq0$ implies CSB.

Substitution of Eq. (10) into Eq. (19) yields

$$(1+\varepsilon_t)=F_n(^3\text{H})F_n(^3\text{He})/F_p(^3\text{H})F_p(^3\text{He})\ . \tag{20}$$

Furthermore, substitution of Eq. (19) into Eq. (18) and taking $\alpha_t(^3\text{He})=1$ yields

$$Q=1+0.9\varepsilon_t\ . \tag{21}$$

Our data for Q are given in Table I and yield the values for ε_t given in Table VIII.

We also have the P' ratios, where the prime indicates that the ratios are normalized to π^+d and π^-d elastic scattering,

$$P'(^3\text{H})=\frac{\sigma(\theta)[\pi^-\,^3\text{H}]}{\sigma(\theta)[\pi^+\,^3\text{H}]}\frac{\sigma(\theta)[\pi^+d]}{\sigma(\theta)[\pi^-d]} \tag{22a}$$

and

$$P'(^3\text{He})=\frac{\sigma(\theta)(\pi^+\,^3\text{He})}{\sigma(\theta)(\pi^-\,^3\text{He})}\frac{\sigma(\theta)(\pi^-d)}{\sigma(\theta)(\pi^+d)}\ . \tag{22b}$$

These ratios are shown in Fig. 7 for $T_\pi=142$ MeV. The solid line in this figure is the result of a calculation of the ratio of the cross sections based on the impulse approximation.[1] For this calculation, the proton and neutron matter form factors were taken to be the same. The cal-

TABLE VIII. Results for the CSB parameter γ_t, the ratio of the even-nucleon form factors: $\gamma_t \equiv F_n(^3\mathrm{H})/F_p(^3\mathrm{He})$. Also given are the results for ε_t, the CSB parameter in the ratio of the four form factors $(1+\varepsilon_t) \equiv F_n(^3\mathrm{H})F_n(^3\mathrm{He})/F_p(^3\mathrm{H})F_p(^3\mathrm{He})$.

$-t$ (fm^{-2})	γ_t	ε_t	T_π (MeV)	θ_π (lab) (deg)	θ_π (c.m.) (deg)
0.7	1.03±0.03	+0.04±0.04	142	40	43.5
1.0	1.04±0.03	+0.10±0.05	180	40	44.0
1.3	1.05±0.03	+0.08±0.05	220	40	44.4
2.8	1.05±0.04	+0.08±0.10	142	90	95.4
3.6	1.05±0.03	+0.12±0.08	142	110	115
4.9	1.08±0.05	+0.15±0.11	180	110	115.6

culation was made for $T_\pi = 150$ MeV to better approximate off-mass-shell corrections. Refinements of this calculation will be reported separately.[11]

The superratio provides the cleanest experimental way to test CS because it does not depend on the π^+ and π^- beam calibrations. An extensive analysis of the superratio at $T_\pi = 180$ MeV has been made by Gibbs and Gibson.[12] They use multiple-scattering analysis techniques based on a nonlocal optical potential. The spin-flip amplitude is calculated in the distorted-wave approximation. Various parameters are tested over a large range of values. These include the off-shell ranges, the effective energy, the angle transformation, the Kerman-McManus-Thaler (KMT) factor, absorption, and the Coulomb energy shifts. The differences between the even-nucleon and odd-nucleon radii are treated as variables by rescaling the individual proton and neutron densities obtained from Faddeev-equation calculations. The shape of the density distributions are as given by theory. Since the momentum transfer is relatively small, the basic shape is primarily determined by the radius. Gibbs and Gibson found that the superratio was affected little by large variations of all the model parameters except for the difference in the proton and neutron radii δ. They calculated, for different model parameters, numerous χ^2 comparisons of theoretical and experimental superratios reported here and in Ref. 1 for $T_\pi = 180$ MeV. An example is shown in Fig. 8 for three different values of δ. The result of the χ^2 comparison is

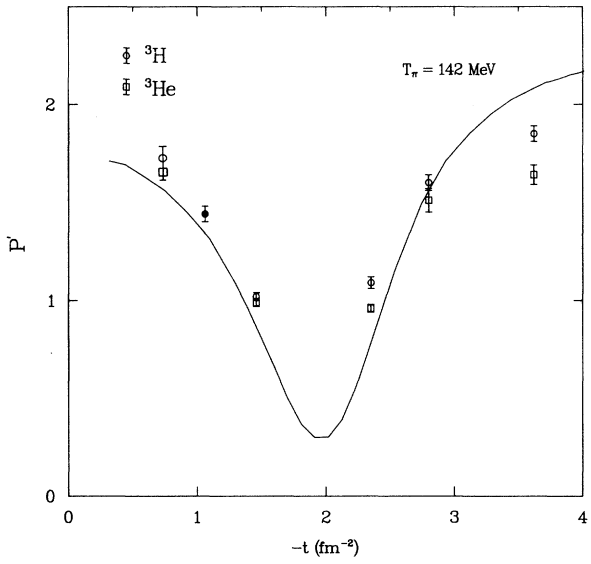

FIG. 7. Ratios of π^+ and π^- cross sections normalized to $\pi^{\pm}d$ scattering:

$$P'(^3\mathrm{H}) = \frac{\sigma(\theta)[\pi^- {}^3\mathrm{H}]}{\sigma(\theta)[\pi^+ {}^3\mathrm{H}]} \frac{\sigma(\theta)[\pi^+ d]}{\sigma(\theta)[\pi^- d]}$$

and

$$P'(^3\mathrm{He}) = \frac{\sigma(\theta)[\pi^+ {}^3\mathrm{He}]}{\sigma(\theta)[\pi^- {}^3\mathrm{He}]} \frac{\sigma(\theta)[\pi^- d]}{\sigma(\theta)[\pi^+ d]} .$$

A data point from Ref. 1 is included (solid symbol). The solid line is an impulse-approximation calculation for $P'(^3\mathrm{H})$.

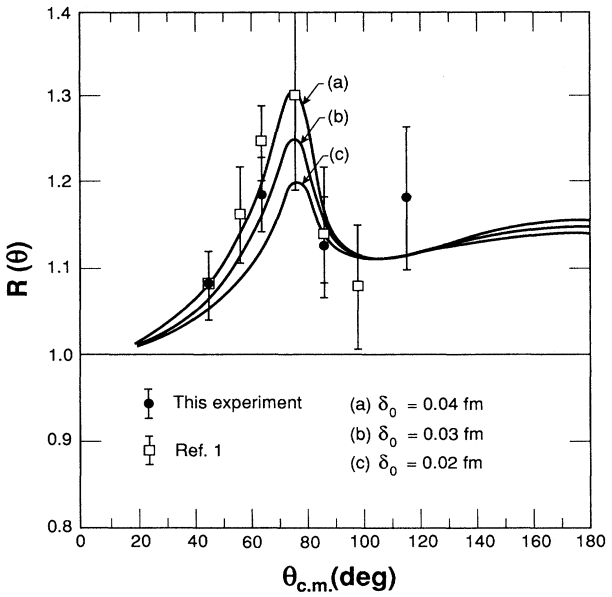

FIG. 8. Sensitivity of the superratio $R(\theta)$ at 180 MeV to a small violation of charge symmetry in the difference of the odd-nucleon radii $\delta_o \equiv r_n(^3\mathrm{He}) - r_p(^3\mathrm{H})$. The model calculations are those of Gibbs and Gibson (Ref. 12). The experimental results are for this and the previous experiment (Ref. 1).

$$\delta_e \equiv r_n(^3\mathrm{H}) - r_p(^3\mathrm{He}) = -0.030 \pm 0.008 \text{ fm} , \quad (23a)$$

$$\delta_o \equiv r_n(^3\mathrm{He}) - r_p(^3\mathrm{H}) = +0.035 \pm 0.007 \text{ fm} . \quad (23b)$$

These results differ markedly from the radius differences calculated for Coulomb interactions alone. Model Faddeev calculations that incorporate charge-symmetry breaking via ρ-ω mixing yield $\delta_e \simeq -0.042$ fm and $\delta_o \simeq +0.027$ fm, consistent with the above values. Thus, Gibbs and Gibson conclude that "a significant charge-symmetry-breaking effect (beyond the Coulomb interaction) has been observed in the difference in the ^{3}H and ^{3}He radii."[12]

The CSB models of Kim, Kim, and Landau,[13] Barshay and Seghal,[14] Kim,[15] and Kim, Krell, and Tiator[16] have already been discussed in Refs. 1 and 10. They do not agree with the data at $T_\pi = 180$ MeV.

C. Model calculations for $\sigma(\theta)[\pi^\pm\,{}^3\mathrm{H} \to \pi^\pm\,{}^3\mathrm{H}]$ and $\sigma(\theta)[\pi^\mp\,{}^3\mathrm{He} \to \pi^\mp\,{}^3\mathrm{He}]$

The four cross sections for π^+ and π^- elastic scattering from ^{3}H or ^{3}He constitute a stringent test for interaction models. Detailed information is available on the electromagnetic form factors for ^{3}H and ^{3}He for making first-order calculations, and Faddeev equations yield realistic ^{3}H and ^{3}He wave functions that include the detailed Coulomb interactions between the two protons in ^{3}He.

The main feature of the differential cross sections in the Δ resonance region is the precipitous falloff with increasing scattering angle up to $\tilde{\theta}_\pi \sim 80°$ c.m. $\sigma(\theta)[\pi^+\,{}^3\mathrm{H}]$ levels off beyond 80° while $\sigma(\theta)[\pi^-\,{}^3\mathrm{H}]$ has the striking NSF dip. These features follow naturally from the relativistic impulse approximation, in which

$$\sigma(\theta)[\pi\,{}^3\mathrm{H}] \sim [|\bar{f}(\pi N)|^2 + |\bar{g}(\pi N)|^2]|F(^3\mathrm{H})|^2$$

and $\bar{f}$ and $\bar{g}$ are the coherent sums of the non-spin-flip and spin-flip πN scattering amplitudes. The matter form factors $F(^3\mathrm{H})$ are expected to be similar to the electromagnetic form factors when the momentum transfer is not too large (and meson-exchange forces do not play an important role).

The falloff in cross section up to $\tilde{\theta}_\pi \sim 80°$ is due to a combination of the falloff in the ^{3}H form factor and the decrease in $\sigma(\theta)[\pi N]$. The NSF dip is a direct consequence of the spin-flip dominance of πN scattering around $\tilde{\theta}(\pi N) = 90°$, which corresponds to $\tilde{\theta}_\pi = 78°$ in the $\pi\,{}^3$H system, when $T_\pi = 180$ MeV together with the spin structure of ^{3}He in which the paired neutrons do not allow single spin flip. For angles $\tilde{\theta}_\pi > 90°$, the impulse approximation is no longer valid because the momentum transfer is too large to be accommodated in a single scattering. Thus, it follows that multiple scattering becomes increasingly important as $\tilde{\theta}$ varies from 90° to 180°, and we expect the cross section to flatten off. That this is apparently the case is shown by our single large-angle data point at $\tilde{\theta}_\pi = 116°$.

The above features also hold at $T_\pi = 142$ MeV as can be seen in Fig. 6(a), including the NSF dip in $\pi^-\,{}^3$H scattering. At $T_\pi = 220$ MeV, this experiment does not have enough data points to see the NSF dip, but we ex-

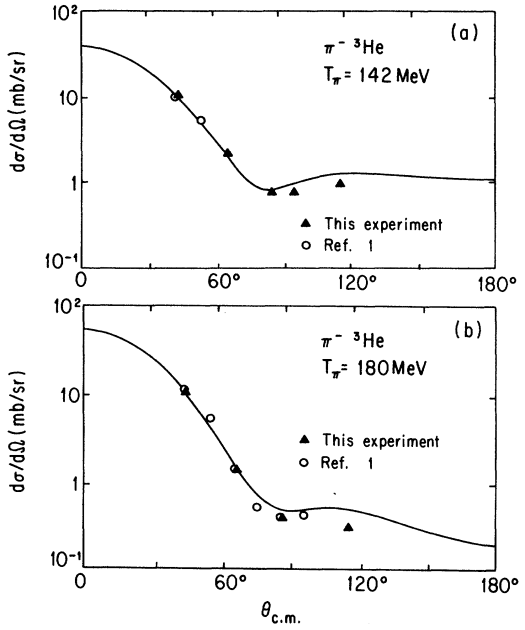

FIG. 9. (a) Model calculation for π^- elastic scattering from ^{3}He by Wakamatsu (Ref. 18) for $T_\pi = 135$ MeV compared with the data at $T_\pi = 142$ MeV. (b) Same as (a) for $T_\pi = 174$ MeV, compared with the data at $T_\pi = 180$ MeV.

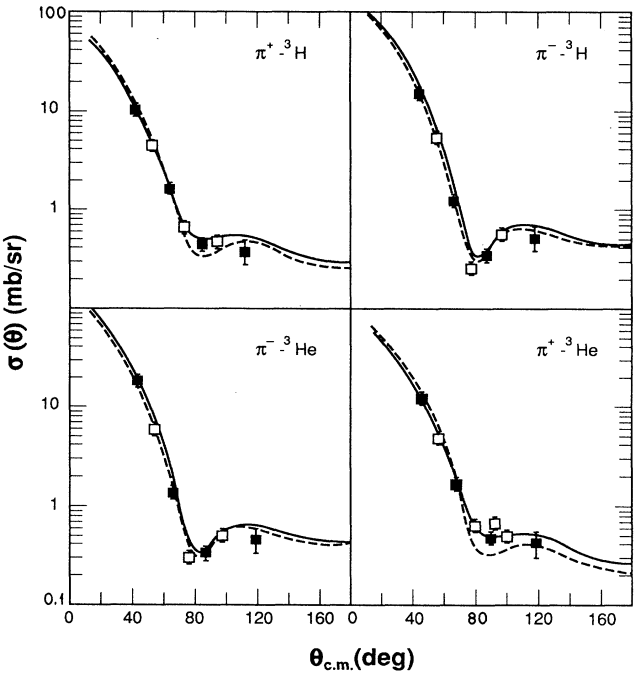

FIG. 10. Model calculation of $\pi^\pm$ elastic-scattering cross section for ^{3}H and ^{3}He by Gibbs and Gibson (Ref. 12) for $T_\pi = 180$ MeV compared with our data (solid symbols) and those of Ref. 1 (open symbols). The two curves represent different sets of input variables discussed in Ref. 12.

pect it to be present. Indeed, our expectation is born out by a recent measurements by our group; a preliminary data point is included in Fig. 6(c). The numerical analysis of the data in terms of neutron and proton matter form factors for ^{3}H or ^{3}He is rather detailed and falls outside the scope of this work.[11]

Previous calculations, such as the ones based on the Laplace and Kisslinger potential model, are discussed in Ref. 17 but their agreement with the data is not acceptable. Reasonable agreement with the differential cross-section features is obtained by Kim, Kim, and Landau,[13] this is not the case for the models of Refs. 14–16.

Wakamatsu[18] has evaluated $\sigma(\theta)[\pi^- {}^3\mathrm{He}]$ based on an optical-model potential in momentum space with second-order effects and nuclear binding corrections. His results at nearby energies are compared with our data in Fig. 9. The agreement is reasonable. The work by Nagaoka and Ohta,[19] based on a multiple-scattering formalism with emphasis on the effects of the Pauli principle, has not been extended to our energies, but the agreement with old $\pi^- {}^3$He data at other energies is not encouraging.

Excellent agreement is obtained with the multiple-scattering model of Gibbs and Gibson[12] as can be seen in Fig. 10. This adds further confidence to their numerical evaluation of the source of CSB based on the superratio.

V. CONCLUSION

We have obtained extensive new data on the charge-symmetric superratio R and simple ratios r_1' and r_2' for π^+ and π^- elastic scattering from ^{3}H and ^{3}He at $T_\pi = 142$, 180, and 220 MeV, spanning the region of the $\Delta(1232)$ resonance. For all three cases, R and r_2' are greater than one, while r_1' is consistent with one. The marked deviation of R from unity indicates a violation of charge symmetry. Models which were constructed to explain $R \neq 1$ with Coulomb effects alone fail to reproduce our results over the full angular range of the measurements.

Gibbs and Gibson[12] have shown that our measurements of the superratio R at $T_\pi = 180$ MeV provide clear evidence of CSB in the radius differences for both the odd and the even nucleons in ^{3}H and ^{3}He. The $\pi^- {}^3$H angular distribution at $T_\pi = 142$ MeV shows a clear NSF dip, already reported to occur at $T_\pi = 180$ MeV. Both $\pi^+ {}^3$H and $\pi^- {}^3$H angular distributions up to $\tilde{\theta}_\pi = 80°$ decrease rapidly with increasing angle, due in large part to the decrease in the ^{3}He form factors; similar behavior is seen for $\pi^+ {}^3$He and $\pi^- {}^3$He scattering.

ACKNOWLEDGMENTS

We greatly appreciate the special effort of J. Van Dyke in designing and testing the tritium target cell. We thank H. R. Maltrud and L. L. Sturgess for help with the gas-handling operation. The assistance of A. M. Petrov in several aspects of the experiment, of S. Graessle and K. Mitchell in taking the data, and of R. Ziock, R. Kessler, and L. Kramer in its analysis is much appreciated. This work was supported in part by the U.S. Department of Energy (DOE) and National Science Foundation under Contracts DE-AS03-81ER40021 and DE-AS05-81ER40036 and Grants DE-FG05-86ER40285 and NSF-PHY-8604524.

*Present address: Los Alamos National Laboratory, Los Alamos, NM 87545.

[1]B. M. K. Nefkens, W. J. Briscoe, A. D. Eichon, D. H. Fitzgerald, A. Mokhtari, J. A. Wightman, and M. E. Sadler, Phys. Rev. C **41**, 2770 (1990).

[2]G. A. Miller, B. M. K. Nefkens, and I. Slaus, Phys. Rep. **194**, 1 (1991).

[3]B. M. K. Nefkens, W. J. Brisoe, A. D. Eichon, D. H. Fitzgerald, J. A. Holt, A. Mokhtari, J. A. Wightman, M. E. Sadler, R. L. Boudrie, and C. L. Morris, Phys. Rev. Lett. **52**, 735 (1984).

[4]H. A. Thiessen, Los Alamos Internal Report LA-6663-MS, 1977 (unpublished); R. L. Boudrie, J. F. Amann, C. L. Morris, H. A. Thiessen, and L. E. Smith, IEEE Trans. Nucl. Sci. **NS26**, 4588 (1979); J. F. Amann, R. L. Boudrie, H. A. Thiessen, C. L. Morris, and L. E. Smith, *ibid.* **NS26**, 4389 (1979); L. G. Atencio, J. F. Amann, R. L. Boudrie, and C. L. Morris, Nucl. Instrum. Methods **187**, 381 (1981).

[5]D. Cochran *et al.*, Los Alamos National Laboratory Report LAMPF SOP No. 130, 1986.

[6]G. R. Smith *et al.*, Phys. Rev. C **38**, 240 (1988).

[7]R. Arndt, J. M. Ford, and L. D. Roper, Phys. Rev. D **32**, 1085 (1985); also R. Arndt, SAID program (unpublished).

[8]K. Gabathuler *et al.*, Nucl. Phys. **A350**, 253 (1980).

[9]C. R. Ottermann, E. Boschitz, W. Gyles, W. List, R. Tacik, R. Johnson, G. Smith, and E. Mathie, Phys. Rev. C **32**, 928 (1985).

[10]C. Pillai, D. B. Barlow, B. L. Berman, W. J. Briscoe, A. Mokhtari, B. M. K. Nefkens, A. M. Petrov, and M. E. Sadler, Phys. Lett. B **207**, 389 (1988).

[11]B. M. K. Nefkens (unpublished).

[12]W. R. Gibbs and B. F. Gibson, Phys. Rev. C **43**, 1012 (1991).

[13]K. Y. Kim, Y. E. Kim, and R. H. Landau, Phys. Rev. C **36**, 2155 (1987).

[14]S. Barshay and L. M. Sehgal, Phys. Rev. C **31**, 2133 (1984).

[15]Y. E. Kim, Phys. Rev. Lett. **53**, 1508 (1984).

[16]Y. E. Kim, M. Krell, and L. Tiator, Phys. Lett. B **172**, 287 (1986).

[17]B. M. K. Nefkens, in *Few Body Systems and Nuclear Forces II,* Vol. 87 of *Lecture Notes in Physics,* edited by H. Zingl *et al.* (Springer-Verlag, New York, 1987), p. 189.

[18]M. Wakamatsu, Nucl. Phys. **A340**, 289 (1980).

[19]R. Nagaoka and K. Ohta, Phys. Rev. C **33**, 1393 (1986).